PAPER

Check for updates

Piezostimulation using ultrasound-active poly-L-lactide films: the effects of a ZnO filler and cold atmospheric plasma surface treatment

Špela Štor, [ID] †[a] Martina Žabčić, [ID] †[a,b] Lea Gazvoda,[a] Masoumeh Sepideh Salehidashtbayaz,[c] Ita Junkar,[d] Tina Radošević,[e] Matejka Podlogar,[e] Martin Šala, [ID] [f] Matjaž Spreitzer [ID] [a] and Marija Vukomanovic [ID] *[a]

Piezostimulation has the potential to promote human cell growth while inhibiting bacterial growth. Antimicrobial action physically destroys the bacterial cell wall without providing bacteria with too many options for developing resistance. However, the mechanism is typically not fast enough to follow the rapid kinetics of microbial growth, and improvement of the efficacy is needed. Here, we show that the synergy of bulk modification with a ZnO filler and surface modification with cold atmospheric plasma leads to a highly functional organic piezoelectric biomaterial. Specifically, the ZnO filler strengthens the piezoelectric response of piezoelectric poly-L-lactide (piezo-PLLA) after its integration into the polymer bulk, whereas the plasma surface treatment changes the surface chemistry and partially reveals integrated ZnO particles on the surface. Both effects significantly affected piezostimulation and improved the interactions with two types of cells. Specifically, the increased content of ZnO NPs in the piezo-PLLA films increased the contact of both bacteria (*E. coli*) and human keratinocytes (HaCaT) with the film surface. Consequently, after activation with ultrasound (1 MHz), the surface very effectively transferred the signal to the adhered cells, which resulted in fast and effective antimicrobial activity. Moreover, for adhered HaCaT cells, stimulation promoted proliferation, cell mobility, intercellular connections and cytoskeleton formation. In combination, these two types of interactions are very important for promoting skin regeneration and wound healing.

Introduction

Piezoelectric stimulation has been recently introduced as a very interesting new approach for designing effective antimicrobial surfaces that are applicable in biomedicine.[1] This is particularly important because the World Health Organization (WHO) has stated that the main drivers in the development of drug-resistant pathogens and therefore the occurrence of anti-

microbial resistance (AMR) are the misuse and overuse of antibiotics in humans, animals and plants. AMR is directly responsible for an enormous number of global deaths, longer and more complicated infections, and riskier surgeries and chemotherapies.[2] In light of alternative antimicrobial actions, piezostimulation acts as a bacterial cell-nonspecific stimulus that disrupts their cell walls, which leads to their death, and therefore presents a promising option.[3]

Among the different piezoelectric materials that have been investigated for providing piezostimulated antimicrobial action,[4] poly-L-lactide (PLLA) is a very good choice. PLLA is a rare organic piezoelectric polymer that combines biodegradability, biocompatibility and production from reusable resources. Its use in biomedicine for various applications, such as tissue regeneration, wound healing and drug delivery systems, is approved by the Food and Drug Administration (FDA) and the European Medicines Agency (EMA).[5] As a tool for providing antimicrobial action, PLLA has been designed in the form of piezoelectric yarn,[6] uniaxially drawn films[5] and films formed of aligned nanotubes.[7] The PLLA yarn was processed as left- or right-handed helical multifibres, which were combined to create a piezoelec-

[a]Advanced Materials Department, Jozef Stefan Institute, Jamova 39, 1000 Ljubljana, Slovenia. E-mail: marija.vukomanovic@ijs.si

[b]Jožef Stefan International Postgraduate School, Jamova 39, 1000 Ljubljana, Slovenia

[c]Biotechnical Faculty, University of Ljubljana, Jamnikarjeva ulica 101, 1000 Ljubljana, Slovenia

[d]Department of Surface Engineering, Jozef Stefan Institute, Jamova 39, 1000 Ljubljana, Slovenia

[e]Nanostructured Materials, Jozef Stefan Institute, Jamova 39, 1000 Ljubljana, Slovenia

[f]National Institute for Chemistry, Department of Analytic Chemistry, Hajdrihova 19, 1000 Ljubljana, Slovenia

†Shared first authorship.

tric textile. Twisting the textile initiated an electrical field, which provided antimicrobial effects.[8] In the case of films, PLLA was either uniaxially stretched or processed into nanotubes using a template.[3] Mechanical stimulation was provided by deforming the polymer using ultrasound (US). In response to US activation, the PLLA film generated a charge that damaged the bacterial membrane.[3] The antimicrobial actions that resulted from US-activated piezostimulation using a drawn PLLA film and a film formed of PLLA nanotubes[3] strongly depended not only on the piezoelectricity of the films but also on the contact between the films and bacteria. Although the action of the PLLA films was bactericidal, the rate of antibacterial action was very slow, which was attributed to poor contact between the bacteria and the surface.[3]

A practical approach for tailoring the piezoelectric properties of PLLA is the addition of morphologically anisotropic fillers.[9] They act as nucleating agents, being piezoelectric or nonpiezoelectric, and consequently affect the crystallinity of PLLA. When the fillers are elongated particles, their morphological anisotropy affects the orientation of the PLLA chains. Many fillers increase one or even both of these characteristics, thereby increasing the piezoelectric response.[9] An interesting choice for the PLLA filler is ZnO nanoparticles (ZnO NP filler). ZnO is stable in various nanoscale morphologies, such as rods, wires, rings, tetrapods, belts, cages, and helices.[10] These particles already exhibit inherent antimicrobial activity, and their morphology, size and surface area play key roles in their antimicrobial activity.[10] This activity is a consequence of several mechanisms, including disruption of the cell membrane, release of Zn^{2+} ions and generation of reactive oxygen species (ROS).[10,11] In addition, ZnO particles have very important effects on local anti-inflammatory activity and skin regeneration.[11,12]

The surface properties of piezoelectric PLLA can be altered by using various chemical approaches, including surface etching.[13] An interesting option is also offered by atmospheric pressure plasma (APP). This approach enables many benefits, such as increased surface roughness and an increased proportion of hydrophilic functional groups. The treatment is localized only to the surface of the PLLA film, whereas the bulk properties of the film and the main PLLA structure remain unchanged.[14]

Two main problems were previously identified as the main reasons for the slow rate of antimicrobial action of US-activated piezostimulated drawn PLLA films: low piezoelectricity and insufficient contact between bacteria and the polymer. Thus, the main aims of this work were (a) to explore the ability of a rod-like ZnO NP filler to affect the structural properties of PLLA drawn films and tailor their piezoelectricity and (b) to modify the surface using plasma to achieve better wettability and improved roughness for better cell adhesion and more effective stimulus transfer. For the first time, US-activated piezostimulation was combined with the effects of a ZnO NP filler and plasma, and their combination was hypothesized to generate interesting synergistic effects and offer an innovative solution for wound healing and skin tissue regeneration.

Experimental

Materials

Poly-L-lactide resomer L 207 S (Evonik), chloroform (≥99.8%, Sigma-Aldrich), *N*,*N*-dimethylformamide (DMF, anhydrous, 99.8%, Sigma-Aldrich), Dulbecco's modified Eagle's medium (DMEM, Sigma-Aldrich), foetal bovine serum (FBS, Gibco), penicillin–streptomycin antibiotics (1 : 1, Gibco), Dulbecco's phosphate-buffered saline (DPBS, Sigma-Aldrich), PrestoBlue cell viability reagent (Molecular Probes, Thermo Fisher Scientific), glutaraldehyde solution (grade I, 25% in H_2O, Sigma-Aldrich), Triton X 100 (Sigma-Aldrich), hexamethyl-disilazane (HMDS, ≥99%, Sigma-Aldrich), Luria-Miller (LB) broth (Carl Roth), agar (powder, Millipore, Sigma-Aldrich), zinc acetate dihydrate ($Zn(CH_3COO)_2 \cdot 2H_2O$, ACS 98.0–101.0%, Alpha Aesar), and lithium hydroxide (LiOH, ≥98%, Sigma-Aldrich) were used.

Processing PLLA/ZnO films with plasma-modified surfaces

Synthesis of a nanorod ZnO NP filler. A nanorod ZnO NP filler (ZnO NPs) was synthesized using $Zn(CH_3COO)_2 \cdot 2H_2O$ as the precursor by following published procedures.[15] Briefly, 32.9 g of the precursor material was dissolved in 500 ml of absolute ethanol under constant stirring in a glass vessel. The mixture was heated to 80 °C, after which 300 ml of condensate was collected and subsequently discarded. The remaining solution was rapidly cooled to room temperature, and the initial volume of 500 ml was restored by the addition of 300 ml of absolute ethanol. Afterwards, 5.0 g of LiOH was added, and complete dissolution was reached using an ultrasonic bath (for 15 min). Subsequently, 40 ml of the prepared ZnO nanodot suspension was transferred into Teflon-lined stainless-steel autoclaves (Parr Acid Digestion Bombs, Parr Instrument Company, USA) with 50% filling. The autoclaves were sealed and maintained at 150 °C for 120 h in an oven. After the solvothermal treatment, the suspension was centrifuged and washed repeatedly (five times) with absolute ethanol. The resulting precipitate was redispersed in 5 ml of Milli-Q water, frozen at −80 °C and freeze dried to prevent the agglomeration of the nanorod ZnO NP filler.

Processing PLLA/ZnO films. ZnO NPs were used as fillers to process PLLA composites with a solvent casting method, which was previously established for barium titanate (BTN) and hydroxyapatite (HAp) fillers.[9] Two grams of PLLA was mixed into 20 ml of chloroform with a magnetic stirrer (Witeg/MSH-20D) at 200 rpm and room temperature overnight until the polymer completely dissolved. Before being added to the polymer solution, different amounts of ZnO (20 mg, 40 mg, 80 mg and 120 mg) were dispersed in DMF with an ultrasonic probe (Mfd. Sun Medisys, Deltasound 1 MHz) (35%, 5 minutes, 2 : 1 pulse ratio). Freshly prepared dispersions were instantly added to the polymer solution, and the mixture was stirred using a magnetic stirrer at a high speed (400 rpm) for the next 10–30 minutes until a homogeneous mixture was obtained. Finally, the mixture was poured into a Petri dish and left overnight, which allowed the solvents to evaporate, thereby

resulting in the formation of PLLA/ZnO composite powders. With the solvent-casting method, composites with concentrations of 1, 2, 4 and 6 wt% ZnO were obtained. They were used as starting materials for processing PLLA/ZnO films that were prepared *via* two key steps, namely, hot pressing and drawing, as previously optimized for pure PLLA films.[5] When the ZnO filler was added, the procedure had to be optimized because of the effect of the filler on the crystallization of the polymer. First, the composite powder was annealed in an oven at 250 °C between two polyimide bands and two thin metallic plates, which was followed by hot pressing at 40 kN for 2 minutes on a manual laboratory press. The films between metal plates were immediately quenched in cold water (10 °C) to prevent excessive crystallization. After this step, nondrawn films or films with a drawing ratio equal to 1 (DR1) were obtained. Second, the DR1 films were placed in a heating oven for 40 minutes at 80 °C and drawn to 5 times their initial length (DR5) with a drawing rate of 40 mm min^{-1} in a drawing machine.

Plasma modification of the film surface. The sample surface was modified using APP with argon. The plasma was introduced onto the surface of each 10×10 mm^2 film through a plasma jet (kINPen IND-Lab). For each side of the film, treatment was carried out for 60 s at a constant voltage of 66 kV, a gas flow rate of 2.0 L min^{-1}, and a distance of 10 mm from the top of the pen to the surface of the sample. The treated films were then used in antimicrobial and biocompatibility tests.

Characterization of the PLLA/ZnO films

X-ray diffraction (XRD) and small-angle X-ray scattering (SAXS). The phase composition and crystallite size were determined with an X-ray powder diffractometer (Bruker AXS D4 Endeavor) using Cu Kα radiation ($\lambda = 1.54$ Å) in the 2Θ range of 10–60° with a step size of 0.04° and a capture time of 7 s per step. Two-dimensional patterns were obtained on a SAXSpoint 2.0 system (Anton Paar, Institute of Biotechnology of the Czech Academy of Sciences, located in the BIOCEV Centre, Czech Republic) that was equipped with a gallium source ($\lambda = 1.34$ Å), a synchrotron, and an Eiger R 1M detector at room temperature in transmission mode. The machine was calibrated beforehand using a silver behenate (AgBH) standard. The sample-to-detector distances for the SAXS measurements were 572 mm and 79 mm. The 2D patterns were converted to 1D using the provided SAXS analysis software. Intensities were measured with a 180 ms frame rate and a 15 s acquisition time. The long period (Lp), which characterizes the lamellar structure, was calculated from the q value of the maximum or shoulder in the SAXS intensity 1D profile using the equation Lp = $2\pi/q_{max}$.

X-ray photoelectron spectroscopy (XPS). The surface chemistry of the films was characterized by X-ray photoelectron spectroscopy (XPS, K-Alpha, Thermo VG Scientific, East Grinstead, UK) using a monochromated Al X-ray source that was operated at 1486.6 eV, 12 kV, and 3 mA. XPS measurements were performed at a pressure of 6.8×10^{-7} Pa. Appropriate charge shifting corrections were performed on the

basis of the C 1s and O 1s peaks at 285.26 and 532.29 eV, respectively. The C 1s and O 1s spectra were analysed using the Spectral Data Processor software (ver. 4.3) provided by XPS International LLC (Mountain View, CA, USA).

Inductively coupled plasma–mass spectrometry (ICP-MS) analysis. For LA-ICP-MS measurements for determining the distribution of ZnO on the surfaces of PLLA/ZnO films, the instrumental setup that was used in this work was composed of a laser ablation system (193 nm ArF* excimer; Analyte G2 Teledyne Photon Machines Inc., Bozeman, MT) that was equipped with a standard active two-volume ablation cell (HelEx II), which included the Aerosol Rapid Introduction System (ARIS; Teledyne CETAC Technologies), for fast aerosol washout. The LA unit was coupled to a quadruple ICP-MS instrument (Agilent 7900x, Agilent Technologies, Santa Clara, CA). The ablation parameters were as follows: laser energy density, 1.23 J cm^{-2}; repetition rate, 200 Hz; beam size, 10 μm – square mask; dosage, 5; and total acquisition time for ICP-MS acquisition, 0.04 s (with the corresponding dwell times for specific nuclides: ^{13}C, 2 ms; ^{66}Zn, 5 ms; and ^{111}Cd, 25 ms). The other parameters were based on model predictions for the fastest possible mapping times, avoidance of aliasing, minimal blur and maximal S/N ratios.[16,17] The ablated material was transported from the ablation cell to the ICP using helium as a carrier gas, and argon was added as a makeup gas before the ICP torch. Data processing and image analysis were performed using the HDIP software package (Teledyne Photon Machines Inc., Bozeman, MT).

Polarized Raman spectroscopy. The molecular orientation of the PLLA within the films was characterized using a polarized Raman spectrometer (NTEGRA Spectra NT-MDT) in the frequency range of 200–3200 cm^{-1} with a polarized 488 nm laser. The data were normalized to the peak at 1454 cm^{-1}, which corresponds to the CH$_3$ bending. To observe the orientation of the crystal structure in the polymer films, the order ratio was determined for the peak that corresponded to the C–COO stretching at 875 cm^{-1} by changing the laser and analyser polarization to observe the peak aligned along the fibre direction (∥) and the peak perpendicular to it (⊥), where the polarization of the analyser is always aligned parallel to the laser polarization. For calculations, the equation $R = (A_{\parallel})/(A_{\perp})$ was used, where R represents the absorbance ratio between the parallel and perpendicular measurements.

Differential scanning calorimetry (DSC). The crystallinity of the PLLA within the films was determined using a NETZSCH STA 449 thermal analyser (Jupiter) for differential scanning calorimetry (DSC) analysis under an Ar/O atmosphere (40/10). A sample was placed in a platinum crucible and heated from 40 °C to 200 °C at a heating rate of 20 °C min^{-1} after temperature calibration under the same conditions.[5] With DSC, the glass transition temperature (T_g), melting temperature (T_m) and cold crystallization temperature (T_c) were determined. The percentage of crystallinity (X_c) was calculated as X_c (%) = $((\Delta H(m) - \Delta H_{cc}))/(\Delta H_{100})$, where ΔH_{100} represents a theoretical value for 100% crystalline PLLA films in the α-crystalline form, which is 93.6 J g^{-1}.

Piezoelectric measurements. The voltage output was measured directly when the films were subjected to a mechanical stimulus using 80 kHz and 1 MHz ultrasound. For that purpose, either an ultrasonic bath (80 kHz, Elma, Elmasonic P) with the films submerged deep in the water or a US probe (Mfd. Sun Medisys, Deltasound 1 MHz) with films connected by contact with a US-conductive hydrogel was used. Before measurement, copper electrodes were placed on the short edges of the films, with respect to the drawing direction, and were connected to cables and impregnated against water intrusion. The cables were routed from a piezo film to a Keysight MSOX3034T oscilloscope to record the signal. Measurements were performed on at least three different films.

Zeta potential measurements. The zeta potential was measured by analysing 2 mg of ZnO in 10 ml of water and 10 ml of DMF using a zeta potential analyser (ZetaPALS, Brookhaven Instruments Corporation). Before the zeta potential measurements were performed, all the samples were sonicated for 5 minutes. The zeta potential was obtained from the electrophoretic mobility.

Water contact angle (WCA) measurements. The WCA was measured with a Theta Lite contact angle meter (Biolin Scientific) at room temperature. For that purpose, the sessile drop method was applied when Milli-Q water droplets (approximately 3 µL) were dropped carefully onto the film surface (10 mm × 10 mm).

Scanning electron microscopy (SEM). The surface morphology of the polymer films was investigated with a scanning electron microscope (SEM-JSM 7600F). The samples were sputtered with gold using a BAL-TEC SCD 005 sputter coater to prevent surface charge and observed under 5 kV.

Antibacterial tests

Microdilution test with ZnO NPs. A microdilution test was carried out with Gram-negative bacteria *Escherichia coli* (*E. coli*, ATCC 25922) to analyse the antimicrobial properties of the ZnO NPs. The *E. coli* culture was grown overnight in LB medium at 37 °C, and on the following day, the optical density (OD) was measured at 600 nm, and a solution with a bacterial concentration of 1×10^5 CFU ml^{-1} was prepared. The initial concentration of the ZnO NPs was 2 mg ml^{-1}. The tested concentrations of ZnO ranged from 100 to 1000 µg ml^{-1}, and each concentration was tested in triplicate. The positive control was *E. coli* in LB medium, whereas the negative control was LB medium. Bacterial growth kinetics were monitored for 24 h at 37 °C, and the OD at 600 nm was measured every 15 min (H1 Hybrid Multimode Microplate Reader, Synergy).

Colony counting method with ZnO NPs. The bacterial viability and bactericidal and bacteriostatic concentrations of the ZnO NPs were determined using the PrestoBlue™ cell viability reagent (10×) (Molecular Probes, Invitrogen, Thermo Fisher Scientific) following a previously optimized method.[18] On the basis of the kinetics of bacterial growth and PrestoBlue-detected bacterial viability, bacteria that were treated with selected concentrations of nanoparticles were serially diluted and plated on LB agar plates. Plating was performed in tripli-

cate; the positive control was nontreated bacteria, whereas the negative control was LB medium without bacteria. The agar plates were incubated for 24 h at 37 °C, after which the colony-forming units (CFUs) were counted, the bacterial concentrations in CFU ml^{-1} were calculated, and the negative logarithmic CFU ml^{-1} reduction ($\log_{10}$(CFU ml^{-1})) was determined.

Ultrasound-stimulated antibacterial activity of PLLA/ZnO films. The test was performed following the ISO22196 standard for testing the antimicrobial properties of plastic and nonporous surfaces.[19] An overnight culture of *E. coli* was grown in LB medium at 37 °C, and the working bacterial concentration was 1×10^5. The films were cut into 1×1 cm^2 samples, with 3 parallel samples for each ZnO concentration. In the 24-well plates, a 10 µL drop of bacterial suspension was added per well and smeared on the film surface. The test was conducted without stimulation and with simulation at 80 kHz (amplitude 30%, 20 min) and 1 MHz (on : off 2 : 18 ms, 1.8 W cm^{-2}, 3 min, DC 10%, PRF 50 Hz). In the case of simulation, the plates were dipped in water (either directly in an 80 kHz water bath or in a Petri dish that was connected to a 1 MHz transducer) using the setup from our previous work.[9] Before being dipped in water, the plates were protected from contamination by wrapping the edges with Parafilm. The samples were incubated for 24 h at 37 °C under high humidity. After incubation, the films were washed with 190 µL of PBS and vortexed to remove potential bacteria from the surface, and PrestoBlue was used to determine bacterial viability. On the basis of the PrestoBlue-detected viability, the bacteria in the PBS that were used for film washing were serially diluted and plated on LB agar plates. The agar plates were incubated for 24 h at 37 °C, after which the number of colonies was counted, and $-\log_{10}$(CFU ml^{-1}) was calculated.

SEM analysis of bacteria on PLLA/ZnO films. To investigate the effects of the material and US on the morphology of the bacteria, samples with bacteria from the antibacterial test were fixed and prepared for SEM using the following procedure. In the first step, 2.5% glutaraldehyde in PBS was added, and the samples were incubated for 2 h at room temperature. After the bacteria were fixed, they were washed with PBS, dehydrated with a series of ethanol dilutions (30%, 50%, 70%, 80%, and 100%), and rinsed for 10 min each and 30 min in absolute ethanol. The last step consisted of incubating the samples in 100% HMDS for 15 min after they were replaced with a new amount and left to air dry.

Release of Zn during 24 hours of incubation. *Ex situ* samples for the determination of metal concentrations were collected after 20 h of incubation of the PLLA/ZnO 6 wt% films at 37 °C and analysed using mass spectrometry with inductively coupled plasma. The samples were diluted prior to measurement to the desired concentration range. To prepare standards, ultrapure water (Milli-Q, Millipore) and ultrapure acids (HNO$_3$ and HCl, Merck Suprapur) were used. Standards were prepared in-house by dilution of certified, traceable, inductively coupled plasma (ICP)-grade single-element standards (Merck Certipur). An Agilent quadrupole ICPMS instrument (Agilent 7900, Agilent Technologies, Santa Clara, CA)

that was equipped with a MicroMist glass concentric nebulizer and a Peltier-cooled, Scott-type spray chamber was used for the measurements.

Solid films were digested prior to the measurements. Briefly, each sample was weighed (approximately 100 mg) and digested using a microwave-assisted digestion system (Milestone, Ethos 1) in a solution of 6 ml of HCl and 2 ml of HNO$_3$. The digested samples were cooled to RT and then diluted with 2% v/v HNO$_3$ until the concentration was within the desired concentration range and measured as described above.

Reactive oxygen species (ROS) formation during US stimulation. ROS generation was detected in 96-well plates with three different concentrations of ZnO NPs with and without US stimulation in PBS buffer. The ROS indicator dihydrorhodamine (DHR) (10 μL per well, 0.1 mM) was added to all the samples before stimulation, after which one group was stimulated using 1 MHz stimulation. PBS was used as a negative control, whereas hydrogen peroxide (H$_2$O$_2$) (5%) that was previously activated for 15 min with UV light was used as a positive control. The samples were incubated for 1 h at 37 °C, and the fluorescence was measured at 490/530 nm Ex/Em for three parallel samples for each concentration.

Interactions with human skin cells

ZnO NP cytotoxicity. A low-passage HaCaT keratinocyte cell line (ATCC PCS-200-011) was defrosted from −80 °C, melted with preheated DMEM, and grown in 6-well plates in full DMEM (DMEM supplemented with 10% FBS and 1% penicillin–streptomycin) until it reached confluency. Cells were subsequently seeded into 24-well plates, where they were grown until they reached confluency. Various concentrations of ZnO, which was previously dispersed in DMEM using an ultrasonic probe, were added to the top of the cells and incubated for 24 h at 37 °C under 5% CO$_2$ (MCO-19AIC(UV)-PE incubator; Panasonic, Japan). After 1 h of incubation with 10 wt% PrestoBlue cell viability reagent, the cell viability was determined by fluorescence measurement at 560/590 nm Ex/Em.

Cytotoxicity of PLLA/ZnO films. HaCaT cells were grown in 6-well plates by following the same procedure as that for testing the effects of the ZnO NPs until they reached confluency. PLLA/ZnO films were cut into 10 × 10 mm^2 samples, with 3 parallel samples for each concentration, and immersed in 300 μL of poly-L-lysine. After that, the samples were washed with DPBS and sterilized in complete DMEM by immersion for one hour. The films were then placed again in the 24-well plates, and 20 000 cells per well were added to the surface of each film in a total volume of 400 μL of DMEM and incubated at 37 °C under 5% CO$_2$ in a cell incubator. After 24 h of incubation, the cytotoxicity was measured by adding 10 wt% PrestoBlue to each well (1 h of incubation, fluorescence (560/590 nm Ex/Em)). Additional controls were cells without any treatment. Three parallel experiments and at least two independent experiments were performed.

Ultrasound-stimulated HaCaT cells on the surfaces of PLLA/ZnO films. After cell viability analysis, cell proliferation on the surfaces of the films was investigated without and with US stimulation at 80 kHz (amplitude 30%, 20 min) and 1 MHz (on : off 2 : 18 ms, 1.8 W cm^{-2}, 3 min, DC 10%, PRF 50 Hz). In the case of simulation, the plates were dipped in water (either directly in an 80 kHz water bath or in a Petri dish that was connected to a 1 MHz transducer) using the setup from our previous work.[9] Before being dipped in water, the plates were protected from contamination by wrapping them with Parafilm.[9] The films were subsequently washed with DPBS, fresh DMEM was added, and the plates that were intended for stimulation were exposed to US. After stimulation, the plates were incubated for 24 h at 37 °C. The next day, cell proliferation was evaluated using PrestoBlue. The cells were washed with DPBS, and fresh complete DMEM was added (400 μL). Cell proliferation was followed for 72 h, with stimulation and cell viability studied every 24 h.

Actin filaments. After proliferation was measured, the cells were washed with PBS, incubated with 3.7% paraformaldehyde for 15 minutes, washed with PBS, permeabilized with Triton X-100 (0.5% solution in DPBS) for another 15 minutes and again washed with PBS. The cells were stained with 4′,6-diamidino-2-phenylindole (DAPI) (5 μL mL^{-1} stock in Hank's balanced salt solution) and rhodamine phalloidin (RP) (1 μL mL^{-1}). RP-stained actin filaments were detected at 584/562 nm Ex/Em, whereas DAPI-stained DNA was measured at 355/346 nm Ex/Em. The films with stained cells were placed on a cover glass and observed under a fluorescence inverted microscope (Eclipse Ti-U inverted microscope, Nikon). Analysis was performed in at least two independent experiments, each of which consisted of three parallel experiments.

SEM analysis of bacteria on PLLA/ZnO films. For SEM analysis, HaCaT cells were fixed and dried on the surfaces of PLLA ZnO films by following the same procedure as that for bacteria.

Statistical analysis

Data are expressed as the mean value ± standard deviation (SD) of 3 parallel results from at least two experiments. The graphs were plotted and statistically analysed using GraphPad Prism software. The statistical analysis included a standard two-way ANOVA test in which $p < 0.05$ was considered to indicate a significant difference.

Results

The aim of this study was to tailor the antimicrobial action provided by US-activated piezostimulation of PLLA films. To achieve this aim (illustrated in Fig. 1), the synergy between a ZnO NP filler (Fig. 1a) and plasma-induced surface modifications (Fig. 1e) was explored for the design of highly functional organic piezoelectric materials. The ZnO NPs were integrated in the first stage of film formation (Fig. 1a–d) such that a homogeneous distribution of rod-like filler particles inside the PLLA matrix could affect the bulk of the piezoelectric material and potentially provide additional interactions with
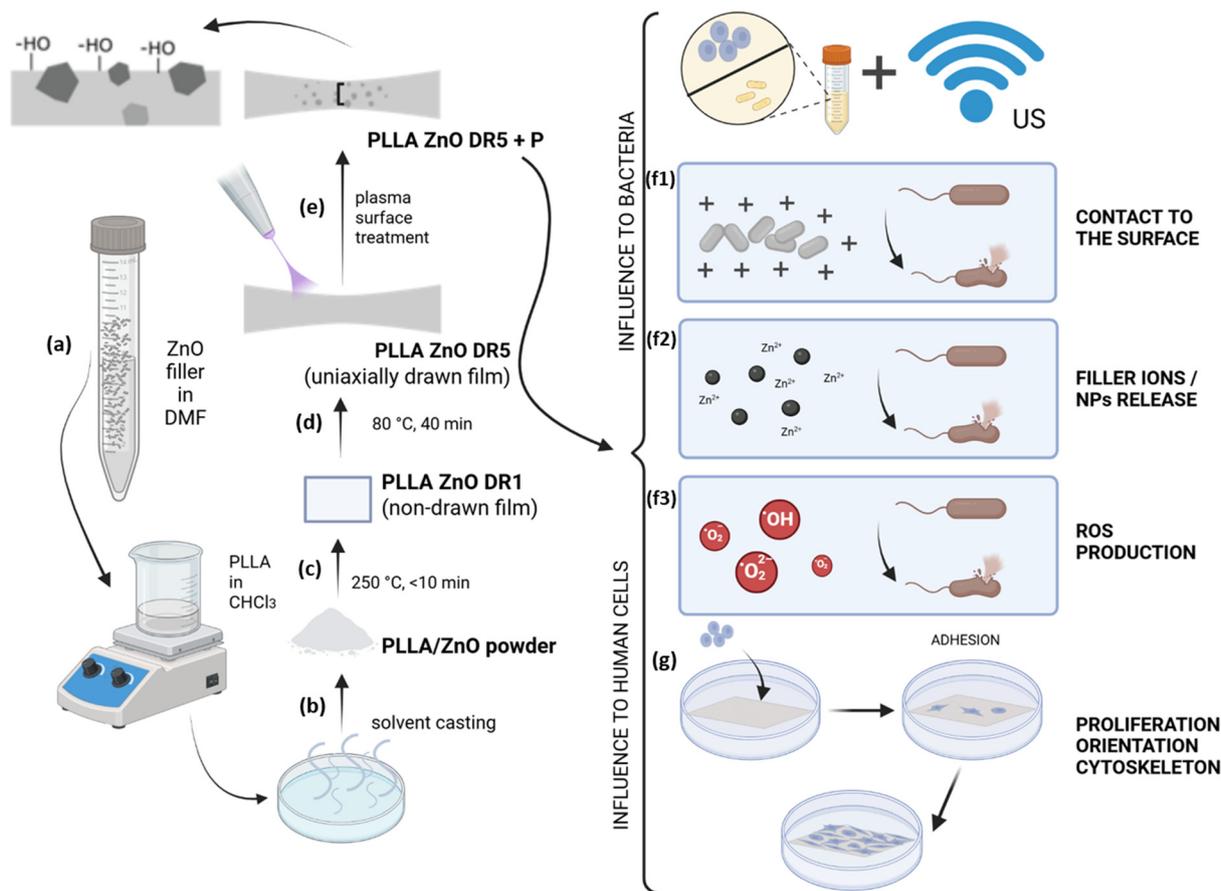
Fig. 1 Main concept of the research: filler modification of PLLA using ZnO (following the introduction of the ZnO NP filler (a) into PLLA to form a PLLA/ZnO composite (b) and its processing into DR5 films (c and d) and surface modification of DR5 films using plasma (e), which introduced new functional groups onto the surfaces of the films and facilitated interactions with cells. The films were mechanically stimulated with US to investigate the effects of piezostimulation on antimicrobial properties against bacteria (f), with consideration of the following possible antimicrobial mechanisms: contact-based (f1), released Zn^{2+} ions (f2), and reactive oxygen species (f3) as well as piezostimulation of human cells (g).

cells. In addition, plasma surface treatment (Fig. 1e), as a final processing step, was used to modify the surface of the piezoelectric PLLA film to improve its contact with cells and achieve more efficient transfer of the stimuli during piezostimulation. These structural and surface modifications were expected to synergistically contribute to the US-induced antibacterial properties of the material (Fig. 1f) and the piezostimulation of human skin cells (HaCaT), thereby leading to better cell proliferation (Fig. 1g). Different antimicrobial mechanisms, including the release of ZnO/Zn^{2+}, generation of ROS and contact effects on the basis of the surface charge of the ZnO NPs, were considered and evaluated (Fig. 1f1–3).

Structural properties of filler-integrated PLLA/ZnO films

Rather than a trend, adding a ZnO filler in a PLLA matrix induced two stages: lower filler content (1 and 2 wt%) and higher content (4 and 6 wt%). Within each of the stages, films had very similar properties. The maximal filler content was 6 wt% and adding more of the filler induced significant polymer rigidity which prevented its drawing. The phase of the

filler particles was identified as the hexagonal ZnO phase (JCPDS: 01-087-8586), with characteristic peaks at $2\Theta = 31.6°$, $34.4°$, $36.2°$, $47.4°$, and $56.7°$, which correspond to the (100), (002), (101), (102), and (110) planes, respectively[20] (Fig. 2a). In addition to the ZnO phase, the XRD patterns of the PLLA/ZnO films show diffraction of the PLLA matrix. Polymer crystallization occurred during the drawing of the DR1 films to DR5. This type of processing most commonly induces the formation of the α′-PLLA phase, with a maximum at 16.4°, which corresponds to the (200) plane.[9] Here, we observed the formation of the α′-PLLA phase in films that were composed of PLLA. However, in the presence of the ZnO NP filler, a more thermodynamically stable α phase, with a peak at $2\theta = 16.8°$, which was attributed to the (110)/(200) plane,[9] also started to form. In addition, the similarity in the intensities of the diffraction maxima that correspond to the filler in the XRD patterns of the ZnO powders and PLLA/ZnO films confirms the absence of particle orientation. The 2D SAXS data show differences in beam scattering, thus indicating filler-induced differences in the PLLA structure (Fig. 2b). The bare PLLA films had minimal
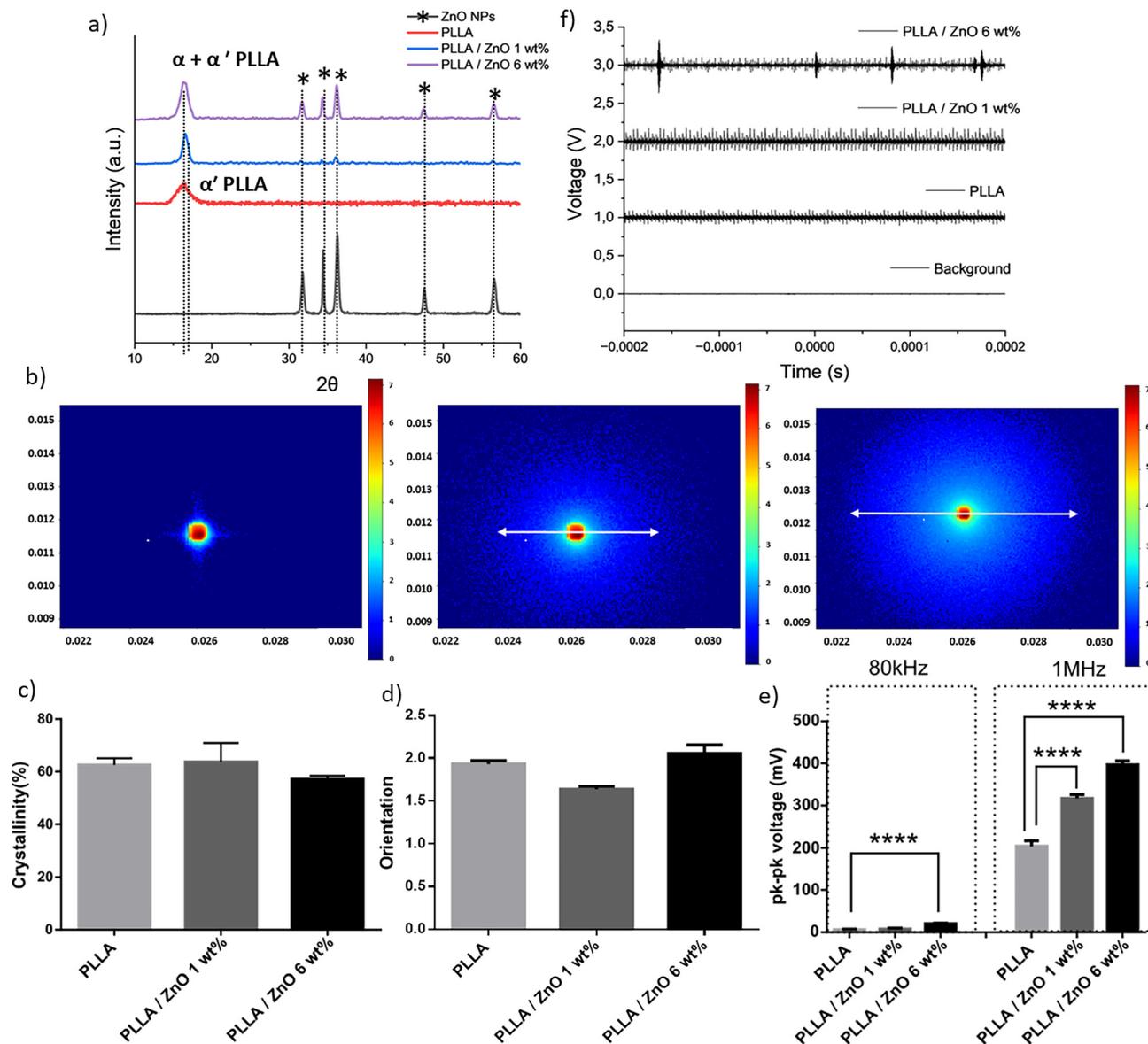
Fig. 2 Structural and piezoelectric characteristics of PLLA/ZnO films: phase compositions of films and fillers (a); 2D SAXS images for PLLA films without and with ZnO NP fillers (b); DSC-determined crystallinity of PLLA in films without and with ZnO NP fillers (c); effect of fillers on the orientation of the films (d); piezoelectric responses of the films after activation with 80 kHz– and 1 MHz US stimulation (e); and piezoelectric signal that was obtained during 1 MHz US stimulation (f). Statistical analysis was performed relative to PLLA without fillers, with $n = 3$; **** refers to $p < 0.0001$ for comparisons PLLA 80 kHz *vs.* PLLA ZnO 6 wt% 80 kHz; PLLA 1 MHz *vs.* PLLA ZnO 1 wt% 1 MHz and PLLA 1 MHz *vs.* PLLA ZnO 6 wt% 1 MHz.

scattering around the central beam, which indicated low long-range ordering.

Once the filler was inside, the scattering intensified and consequently increased with increasing filler content, which indicated a filler-induced increase in long-range ordering. The absence of long-term maxima was caused by the small difference in the density of the amorphous and crystalline α′ PLLA phases. In contrast, the α-PLLA phase had a higher density and therefore showed long periods in SAXS. This finding supports that the ZnO filler induced the formation of a more arranged α-PLLA phase, as identified by XRD phase analysis. However, the absence of long-range ordering does not imply

the absence of lamellae, as has been clearly proven in previous studies.[21,22] Diffused rings that were observed in the 2D SAXS images appear as shoulders in the 1D-extracted graph (Fig. S1) and indicate long-range lamellar ordering. Long-range structures include repeating crystalline and amorphous domains.[23] Adding the ZnO NP filler not only promoted the crystallization of PLLA into a more arranged α phase but also affected lamellar ordering. The peak maximum shifted from 0.38 nm^{-1} for 1 wt% PLLA ZnO to 0.33 nm^{-1} for 6 wt% PLLA ZnO films, which corresponded to an increase in the long periods from approximately 16.38 nm to 18.77 nm. Similar crystallite sizes in PLLA films have been detected earlier as well.[21–23]

The influence of the filler on the crystallization and structural properties of the polymer was investigated using thermal analysis and polarized Raman spectroscopy. As determined by DSC (Fig. 2c), the crystallinities of PLLA, 1 wt% PLLA/ZnO and 6 wt% PLLA/ZnO were very similar. The observed differences were not statistically relevant, and the use of ZnO NPs as a filler did not strongly influence the total crystallinity of the PLLA matrix. Similar results were obtained for molecular chain orientation. The chain orientation of PLLA was determined using polarized Raman spectroscopy (Fig. 2d). The orientation was calculated as the ratio of the intensities of the peaks that corresponded to C-COO groups (875 cm^{-1}) (as relevant structural dipoles) measured parallel and perpendicular to the film drawing direction.[9] All the results were normalized to the appropriate peak that corresponded to CH$_3$ groups (1453 cm^{-1}), whose intensity was constant in both directions. However, the molecular orientation was not significantly affected by the presence of the filler (Fig. 2c).

The presence of ZnO NP fillers in the PLLA matrix and their contributions to the structural properties of the polymer significantly affected its piezoelectric response ($p < 0.0001$) (Fig. 2e). A comparison of the measured piezoelectric responses that were generated by films without and modified with 1 and 6 wt% ZnO revealed that the addition of filler particles increased the piezoelectric response of the PLLA (Fig. 2f). After activation with US, with a frequency of 80 kHz or 1 MHz, the highest response was detected for 6 wt% PLLA/ZnO because it had the highest concentration of the ZnO filler (Fig. 2e).

Surfaces of plasma-modified fillers that contained PLLA/ZnO films

The surface properties of the films were affected by the processing procedure, including both film drawing and surface modification with plasma. According to the results of the XPS analysis (Fig. 3a), slightly higher concentrations of zinc were detected on the surfaces of the drawn films (PLLA/ZnO 1 wt% DR5) than on the surfaces of the films that were obtained after hot pressing (PLLA/ZnO 1 wt% DR1). This confirms that stretching partially exposes the ZnO NP filler to the surface of the film. Detection of zinc contents before and after plasma treatment revealed significantly greater differences. Much more ZnO remained available at the surfaces of the films when they were treated with plasma (PLLA/ZnO 1 wt% + P DR5 and PLLA/ZnO 6 wt% + P DR5). This was a direct consequence of the surface etching that was induced by the plasma, which partially removed the polymer and exposed particles of the filler at the surface.

Another important contribution of the plasma to the surfaces of the films was a change in wettability. On the basis of the water contact angle (WCA) measurements (Fig. 3c and d), plasma treatment induced a significant reduction in the WCA, which changed the wettability of the films from hydrophobic to hydrophilic. Interestingly, increasing the content of the ZnO NP filler increased the hydrophobicity of the PLLA matrix. Consequently, the WCAs of the films with higher contents of the ZnO NP filler decreased only slightly after the plasma treatment (Fig. 3c). As the ZnO NP filler is initially highly hydrophilic (Fig. S2), the observed effect could be assigned to interactions between ZnO NPs and the PLLA matrix which contribute to reorganisation of polymeric functional groups and affect surface chemistry after plasma treatment. Therefore, the wettability of the surface was a combination of the plasma-modified chemistry of PLLA and the ZnO NP filler at the surface interacting with the PLLA matrix.

Morphologically, the filler ZnO NPs were small rods (Fig. 3e) that were 20 nm wide and had lengths that ranged from 40 to 170 nm. The cross-sections of the PLLA, PLLA/ZnO 1 wt% and PLLA/ZnO 6 wt% films (Fig. 3f1–3, respectively) revealed a layered polymeric matrix oriented in the drawing direction. At lower concentrations, larger aggregates of ZnO NP fillers inside the matrix were not observed. The distribution of ZnO NP fillers that were available at the surface and close to the surface of the PLLA films was very homogeneous, as detected by ICP-MS (Fig. 3b). The distribution was also investigated after plasma treatment. For this purpose, EDS analysis was performed on the surfaces of the PLLA/ZnO 6 wt% DR1, PLLA/ZnO 6 wt% DR5 and PLLA/ZnO 6 wt% + P films (Fig. S3). As previously detected by XPS, stretching DR1 onto the DR5 film exposed some of the ZnO NPs to the surface. The effect was more pronounced after the plasma treatment, which additionally exposed the NPs to the surface; however, as they remained partially covered with the PLLA matrix, their distribution at the surface remained homogeneous.

Antibacterial properties

The free ZnO NPs had a modest antibacterial effect on *E. coli* (Fig. 4). Applying ZnO NPs at concentrations that ranged from 100 to 1000 μg ml^{-1} effectively inhibited bacterial growth (Fig. 4a). Bactericidal activity (reduction of at least 99.9% ($\geq$3 log$_{10}$(CFU ml^{-1})[11]) was observed for concentrations higher than 300 μg ml^{-1} (Fig. 4b and c), which corresponded to $\geq$4 log$_{10}$, whereas concentrations of 200 μg ml^{-1} and lower were bacteriostatic. In addition, the antimicrobial activity was tested for Zn^{2+} ions (dissolved from ZnCl$_2$) and the results showed very similar trends to ZnO NPs (Fig. S4).

The contribution of the antimicrobial effect of ZnO NPs as a filler to the total antimicrobial action of the PLLA/ZnO NP films was evaluated in terms of the filler-related active components that are responsible for antimicrobial action. This included testing the generation of reactive oxygen species (ROS) (Fig. 4d) as well as the release of zinc from the PLLA/ZnO NP films (Fig. 4e). The production of ROS that was induced by different concentrations of ZnO NPs was significantly lower than that induced by the positive control (H$_2$O$_2$) and was at the level that was detected for PBS, which was used as a negative control (Fig. 4d). Very similar ROS levels were also detected when the particles were activated with US. This led to the conclusion that ROS production is not high enough to contribute to the antimicrobial activity of ZnO NPs when they are used as fillers in PLLA/ZnO films.
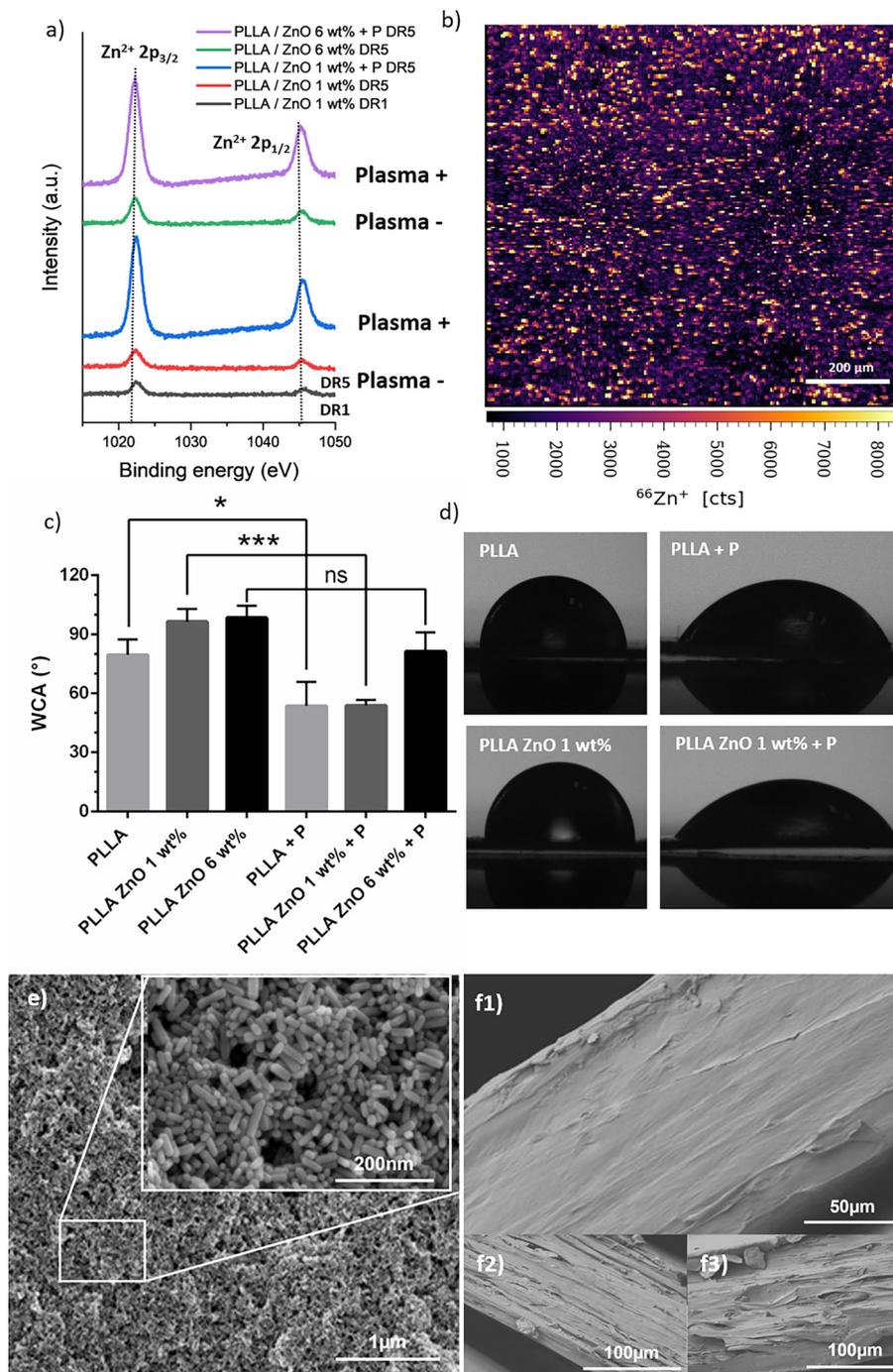
Fig. 3 Surface properties of plasma-modified PLLA/ZnO films. XPS spectra that correspond to zinc at the surfaces of the films before and after plasma treatment, which confirm the increase in the zinc content that was available at the surfaces after modification with plasma (a); ICP-MS mapping of the surface of the PLLA/ZnO 6 wt% film, which shows the distribution of zinc over the surface (b); WCAs for PLLA, PLLA/ZnO 1 wt% and PLLA/ZnO 6 wt% with and without plasma treatment (c); water drops on the surfaces of the PLLA and PLLA/ZnO 1 wt% films, which illustrate a plasma-induced increase in surface wettability (d); SEM images of ZnO NPs (e) and cross-sections of PLLA (f1), PLLA ZnO 1 wt% (f2) and PLLA ZnO NP 6 wt% (f3); P indicates films treated with plasma; statistical analysis was performed for P+ and P− pairs, with $n = 3$, PLLA vs. PLLA + P, $p = 0.0184$; PLLA ZnO 1 wt% vs. PLLA ZnO 1 wt% + P, $p = 0.0003$.

Furthermore, we measured the release of zinc from the films. With ICP analysis, we determined the initial amount of zinc that was present in the PLLA/ZnO 6 wt% film and confirmed that 24 h after incubation in PBS at 37 °C, up to 50 μg ml^{-1} of zinc was released. Considering the modest antimicrobial action of the ZnO NPs, the amount of released zinc was not enough to induce a bacteri-cidal effect.
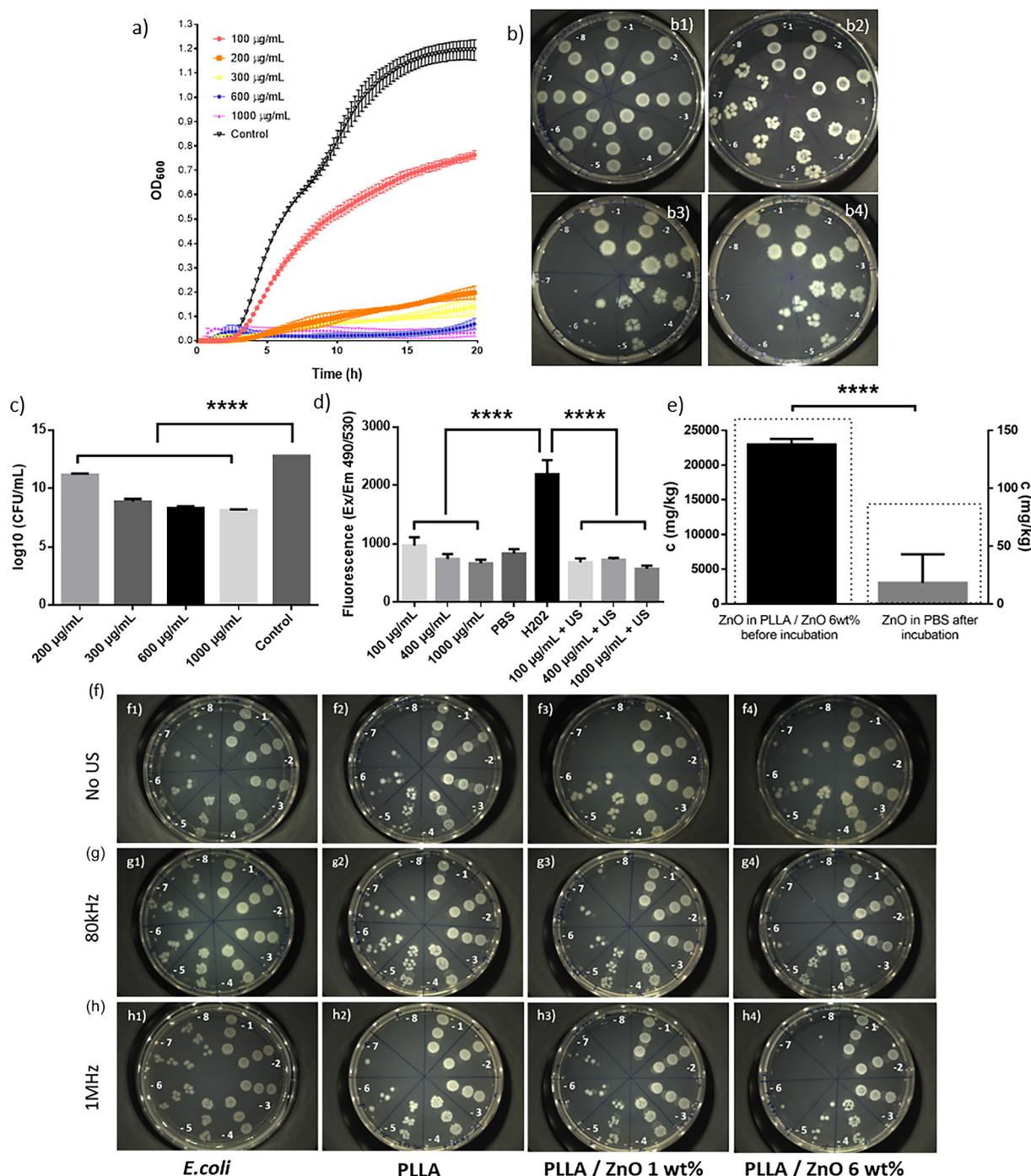
Fig. 4 Antibacterial properties of the ZnO NPs. Kinetics of *E. coli* growth in the presence of 100 μg ml^{-1}, 200 μg ml^{-1}, 300 μg ml^{-1}, 600 μg ml^{-1}, and 1000 μg ml^{-1} of ZnO NPs and without ZnO NPs as a control (a); serial dilutions for colony counting for the positive control of *E. coli* (b1), 200 μg ml^{-1} (b2), 600 μg ml^{-1} (b3) and 1000 μg ml^{-1} (b4) ZnO NPs; *E. coli* log$_{10}$(CFU ml^{-1}) reduction for various concentrations of ZnO NPs (statistical analysis was performed on log$_{10}$(CFU ml^{-1}) reduction compared to the control, with $p < 0.0001$ for all tested concentrations) (c); ROS production for various concentrations of ZnO NPs with and without stimulation with ultrasound, where the negative control was PBS and the positive control was H$_2$O$_2$ (the statistical analysis was performed to compare the ROS levels that were produced by different concentrations of ZnO NPs to the ROS levels that were produced by H$_2$O$_2$, with $p < 0.0001$ for all concentrations) (d); the amount of ZnO in the PLLA/ZnO 6 wt% film before incubation in PBS (mg kg^{-1}) and the total amount of zinc that was released from the PLLA/ZnO 6 wt% film after 24 h of incubation in PBS at 37 °C (mg kg^{-1}) (statistical analysis was performed on the difference between the total and released zinc, $p < 0.0001$) (e); and serial dilutions and colony detection of *E. coli* on films with different concentrations of the ZnO NP filler, with and without piezostimulation (activation with 80 kHz or 1 MHz US) (f–h); in all cases for statistical analysis, $n = 3$, **** refers to $p < 0.0001$.

The contribution of ZnO to the improvement in the antimicrobial properties of the PLLA films was then evaluated on the basis of the charge of their surfaces. The zeta potential of the ZnO NPs was found to be +24.70 ± 1.51 mV in an aqueous environment. The positive potential points to cationic ZnO, as detected earlier.[11,24] This information revealed the potential of ZnO NP fillers to provide contact-based antimicrobial effects that are induced by surface changes. A similar action has been reported in the case of cationic amino acid-functionalized gold nanoparticles.[25]

Additional examination of the antimicrobial effects of the PLLA films with and without ZnO fillers included piezostimulation that was induced by film activation using 80 kHz or 1 MHz US (Fig. 4f). Initially, without stimulation with US, the growth of *E. coli* treated with the surfaces of PLLA, 1 wt% PLLA/ZnO and 6 wt% PLLA/ZnO was very similar, and 1–2 log (CFU ml^{-1}) reductions were observed for films with fillers that were not significantly bactericidal (Fig. 4f1–4). The application of US activation at both 80 kHz and 1 MHz US frequencies improved the antimicrobial activity of the film (Fig. 4g and h). In the absence or presence of low contents of the ZnO filler, the US-activated films showed low inactivation of bacteria, which improved in the case of the combination of US acti-

vation and a high content of the filler. Compared with that of the control, the log(CFU ml^{-1}) significantly decreased for 6 wt% PLLA/ZnO, which was the only case in which a clear bactericidal effect was confirmed (Fig. 4g3 and h3).

However, morphologically, we found that plasma modification initially affected the shape of bacteria that were attached to the surfaces of films with or without ZnO fillers (Fig. 5a1–3).

In the case of activation with 1 MHz US, the bacteria sensed the stress, which was morphologically detected as the initiation of extracellular fibre-like matrix formation, particularly on the surfaces of the PLLA films without the ZnO filler (Fig. 5b1). The presence of ZnO in films that were activated with US induced initial damage to bacterial cells, which increased with increasing ZnO content (Fig. 5b1–3). When combined, plasma modification of the film surface and its activation with US synergistically induced damage to bacterial cells (Fig. 5c1–3). Bacterial cells with severely damaged bacterial walls were detected for the PLLA films and films with ZnO NP fillers.

Interactions with human cells

The cytotoxicity of the ZnO NPs was evaluated in human keratinocytes (HaCaT cells) (Fig. 6a). On the basis of the metabolic
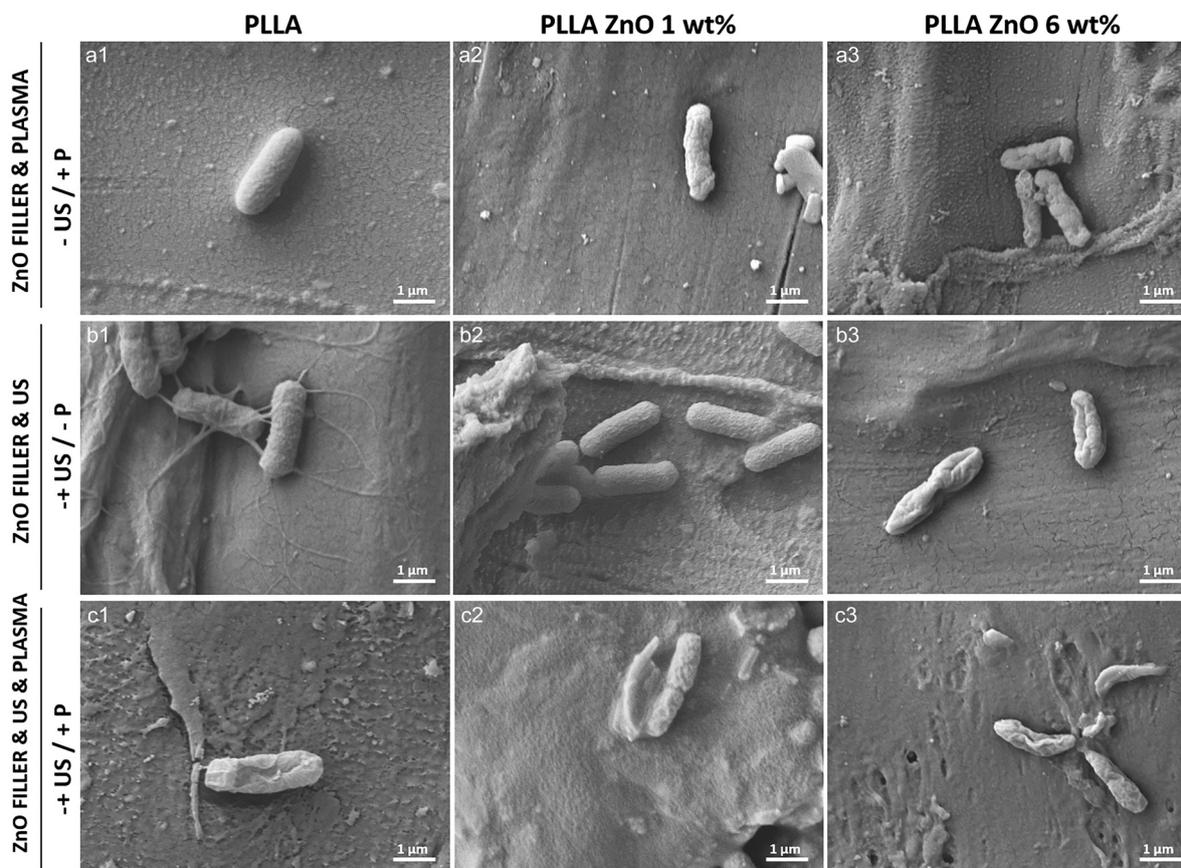

Fig. 5 SEM analysis of bacteria on different surfaces: morphology of bacteria on films that were treated with plasma (a1–a3), activated with 1 MHz US (b1–b3) and synergistically treated with plasma and activated with 1 MHz US (c1–c3), for PLLA, PLLA ZnO 1 wt% and PLLA ZnO 6 wt%, respectively.
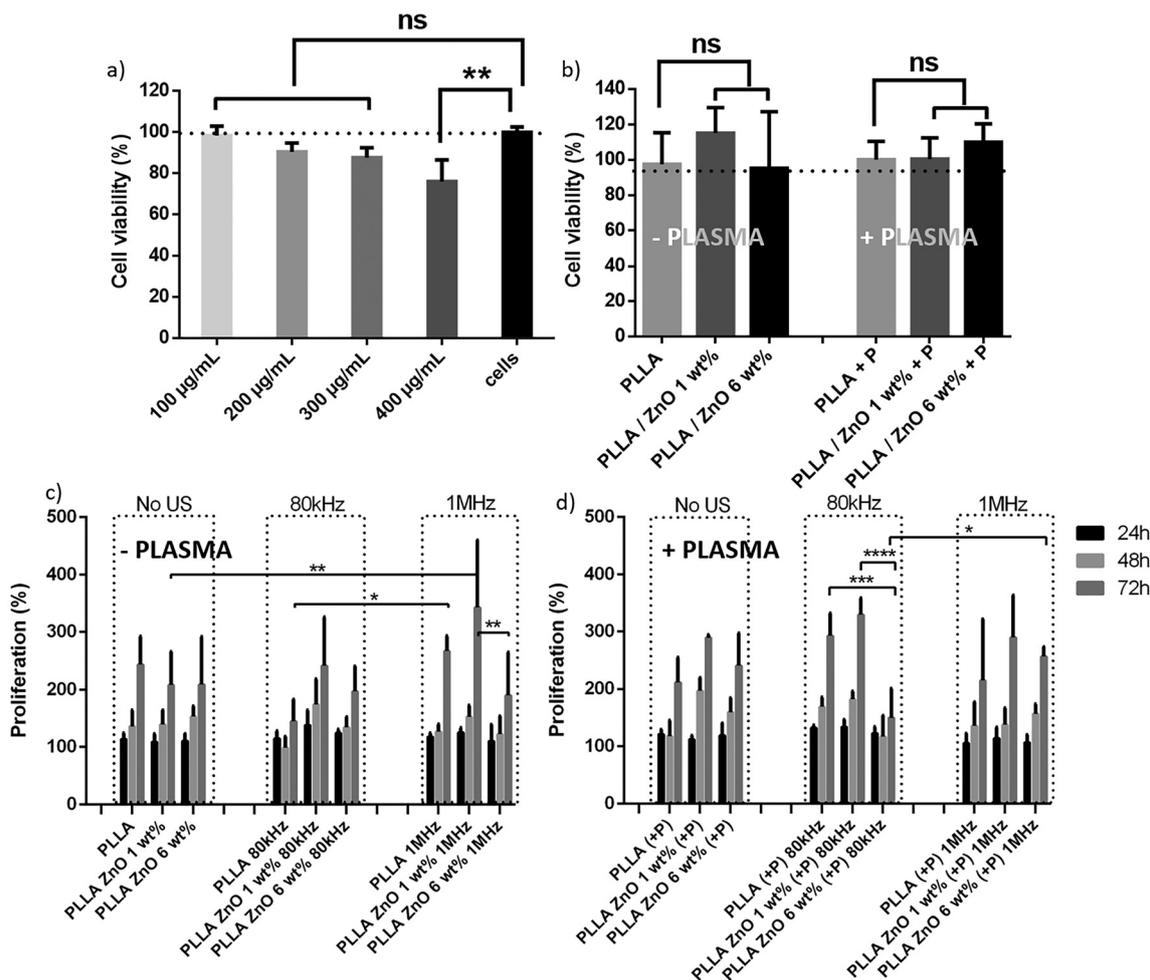
Fig. 6 Cytotoxicity and proliferation of HaCaT cells. Cytotoxicity of ZnO NPs that were tested in the range of $100-400 \ \mu g \ ml^{-1}$ (statistical analysis was performed relative to that of the nontreated cells; ** indicates $p < 0.01$) (a); viability of cells in direct contact with the surfaces of films with and without the ZnO filler before and after surface modification with plasma (b); the proliferation of cells on the surfaces of the PLLA, PLLA/ZnO 1 wt% and PLLA/ZnO 6 wt% films with and without activation (US, 80 kHz and 1 MHz) (PLLA ZnO 1 wt% no US *vs.* 1 MHz $p = 0.0092$; PLLA 80 kHz *vs.* PLLA 1 MHz $p = 0.0272$; PLLA ZnO 1 wt% *vs.* PLLA 6 wt% $p = 0.0021$) (c); and cell proliferation on plasma activated surfaces of the PLLA, PLLA/ZnO 1 wt% and PLLA/ZnO 6 wt% films with and without activation with US (US, 80 kHz and 1 MHz) (PLLA 80 kHz *vs.* PLLA 6 wt% 80 kHz $p = 0.0004$; PLLA ZnO 1 wt% 80 kHz *vs.* PLLA ZnO 6 wt% 1 MHz $p = <0.0001$; PLLA ZnO 6 wt% 80 kHz *vs.* PLLA ZnO 6 wt% 1 MHz $p = 0.0168$) (d).

activity measured using resazurin, particle concentrations lower than $400 \ \mu g \ ml^{-1}$ did not affect cell viability, whereas higher concentrations induced a statistically significant decrease in the number of viable cells ($p < 0.01$), and the particles were considered to be cytotoxic.

Following the cytotoxicity analysis of the filler particles, the highest concentration of ZnO NPs in the films was limited to 6 wt% relative to that in the PLLA matrix. Films with different contents of fillers (PLLA without fillers, PLLA/ZnO 1 wt% and PLLA/ZnO 6 wt%) before and after pretreatment with plasma were tested for cytotoxicity using the same approach (Fig. 6b). None of the films decreased the viability of the cells, and statistically significant differences were not detected as a consequence of increasing the filler content or surface activation using plasma. The cells that directly adhered to the surfaces of the films were tested for proliferation (Fig. 6c and d). For that

purpose, the films with different contents of ZnO NP fillers were activated at 80 kHz or 1 MHz and compared to the corresponding cases when activation was not applied (Fig. 6c). The same set of samples was tested for the case in which the films were pretreated with plasma (Fig. 6d).

In the case of the films without plasma activation, the cell growth on the films that were not activated with US was the same regardless of the presence of fillers. Activation using US particularly increased the proliferation rate for 1 wt% PLLA/ZnO. Although an increase was detected for the case of a low content of the filler (PLLA/ZnO 1 wt%), a higher filler content did not result in any particular difference. The proliferation rate was more strongly promoted by activation using 1 MHz US. When the films were pretreated with plasma, the cell proliferation rate generally increased compared with that of the same film without plasma treatment.

The effects of the filler, US activation and plasma pretreatment on the cytoskeleton, *via* detection of actin filaments, were evaluated in the cells that proliferated on the surfaces of the PLLA films (Fig. 7). The cells, attached on films without plasma treatment and before activation with US, were low in density and naturally rounded in shape (Fig. 7a1–3). We observed an increased number of rounded cells on non-treated films and accordingly detected actin filaments within them. When the surface was pretreated with the plasma, the effect was the same, thus resulting in the formation of rounded cells, but their number on the films clearly

increased and they were growing closely packed one next to another (Fig. 7b1–3). After activation with US, the cells on the surfaces of the films started to polarize and form elongated shapes, with a particular increase in actin filament elongation, but their covering of the surface remained low and did not increase markedly in the presence of the filler (Fig. 7c1–3). In the final case, when US activation was performed on the surfaces of the plasma-pretreated films, a higher number of morphologically polarized, elongated cells, tightly packed and with elongated actin filaments, was observed (Fig. 7d1–3).
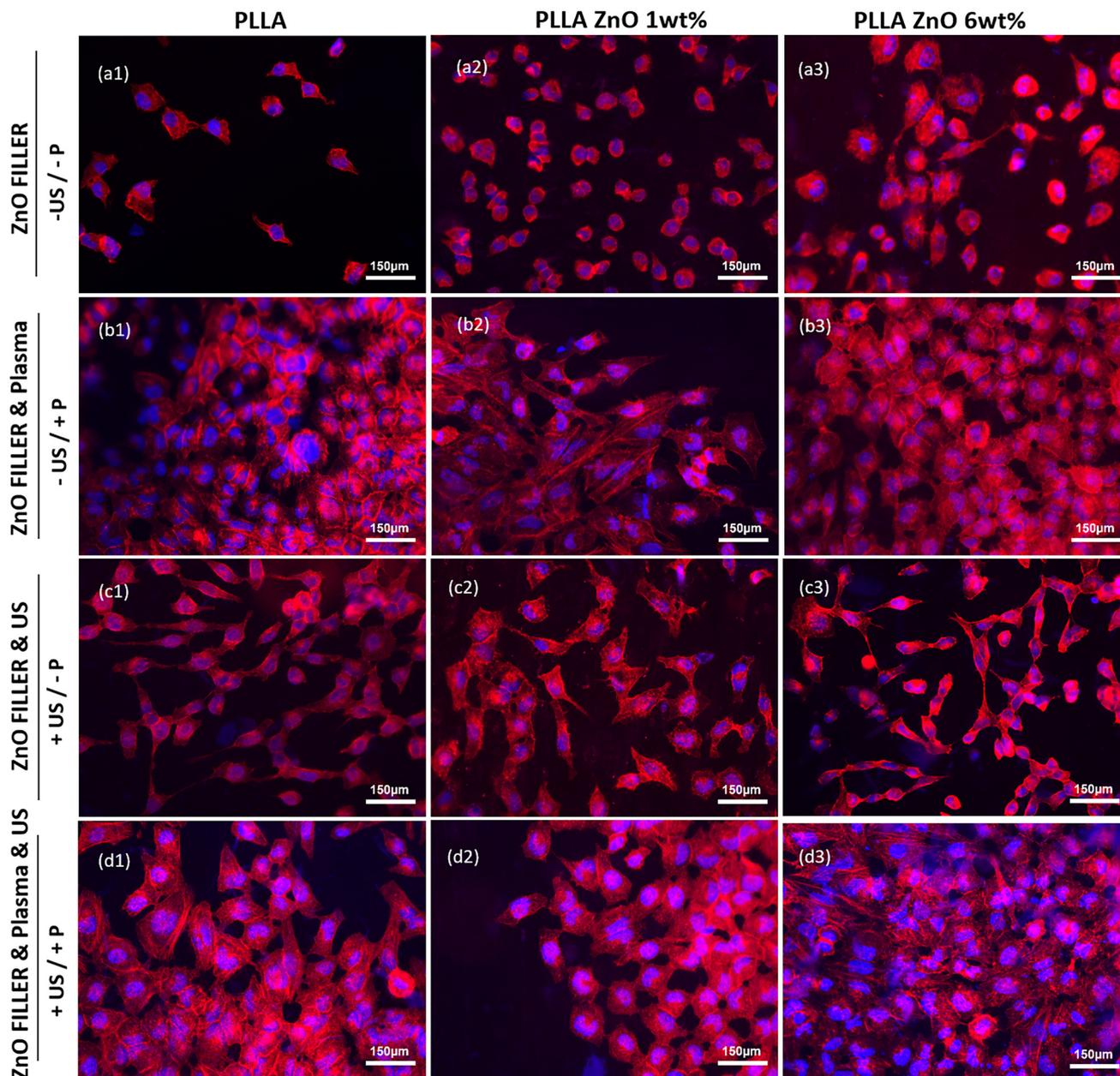

Fig. 7 Effects on actin filament formation in HaCaT cells. Actin filaments in cells on the surfaces of PLLA, PLLA ZnO 1 wt% and PLLA ZnO 6 wt% for the following cases: without any additional treatment (a1–a3), films pretreated with plasma (b1–b3), films activated with US (1 MHz) (c1–c3) and synergy of plasma surface pretreatment and film activation with US (1 MHz) (d1–d3).

Morphologically, the HaCaT cells that adhered directly to the surface of the piezo PLLA ZnO films were characterized by very interesting surfaces (Fig. 8). The piezostimulating cells that adhered to the films, after their activation with US, exhibited very high roughness at their surfaces, thereby resulting in the formation of numerous cellular protrusions in the form of filopodia and lamellipodia, which enabled contact among the cells, as well as between the cells and the surfaces of the films (Fig. 8b). When the surfaces of the films were pretreated with plasma, in addition to the attachment of cells to the films, cell–cell attachment was promoted (Fig. 8c).

Discussion

As a method that physically disintegrates the microbial envelope, piezostimulation does not leave many options for bacteria to develop resistance.[4] However, although it causes permanent damage to the microbial envelope, which leads to microbial death,[3] the mechanism of piezostimulated antimicrobial activity is very slow in comparison with the fast kinetics of bacterial growth. In this work, this problem was addressed by modifying the surface and structural properties of piezo-PLLA films to improve their interactions with cells and consequently tailor their antimicrobial action (illustrated in Fig. 9).
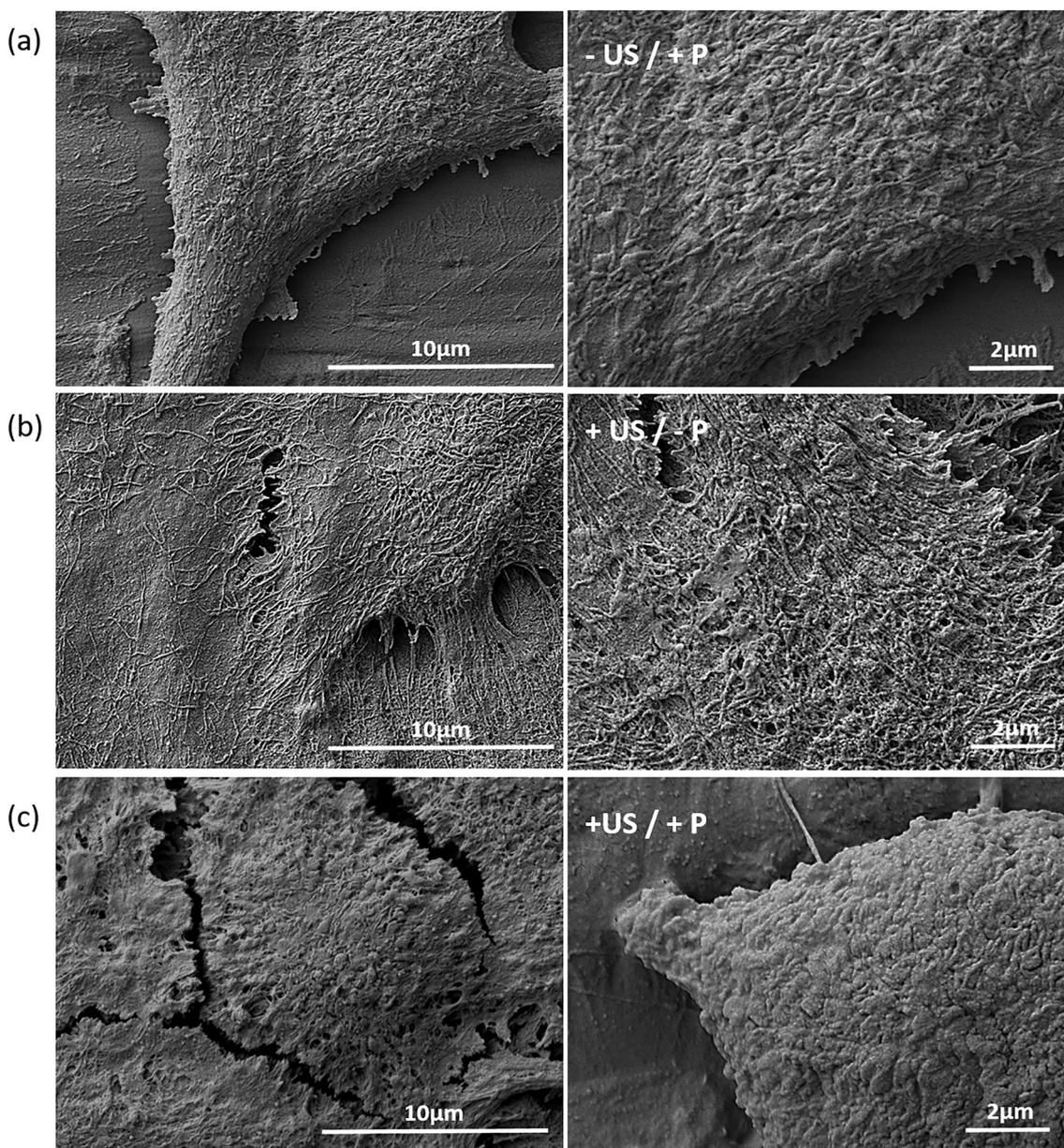

Fig. 8 Cells adhered to the films. SEM images of the morphology of HaCaT cells showing the properties of their surfaces, the formation of filopodia and connections to neighbouring cells after adhesion to films without plasma pretreatment and before activation with US (a), films without plasma pretreatment activated with US (b), and plasma-treated US activated films (c).
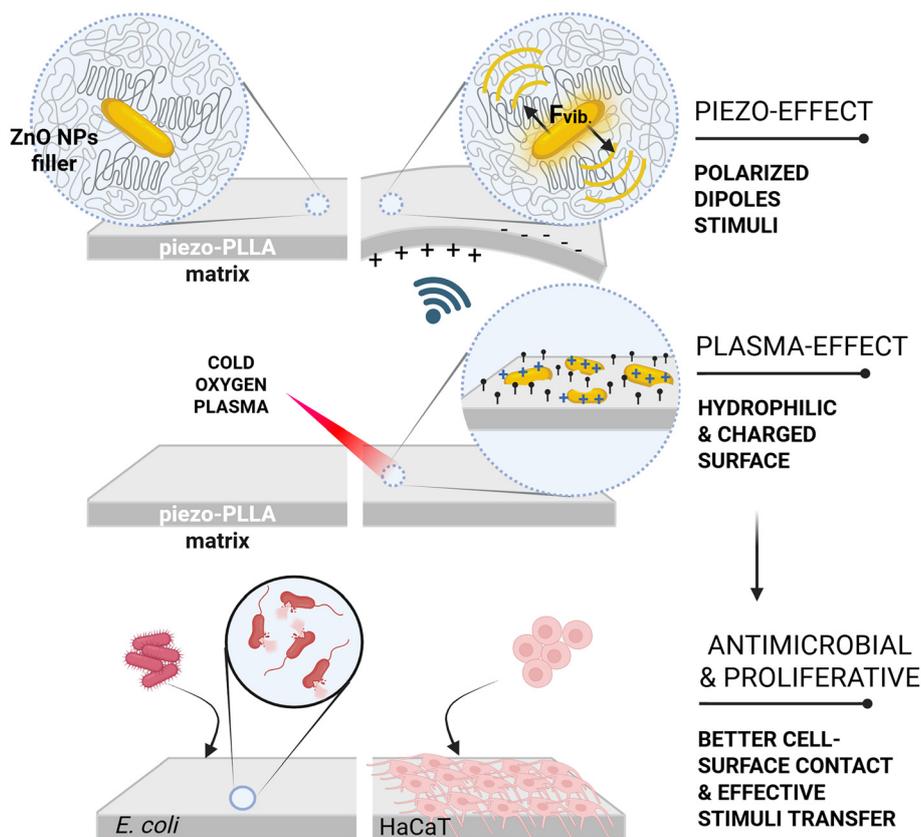
Fig. 9 Illustration of the effects of ZnO NP filler and plasma on piezostimulation: improved piezoelectric response during activation with US, which produces intense stimuli, and a change in the surface chemistry that is induced by surface plasma treatment, which leads to hydrophilic and charged surfaces, both of which induce more effective antimicrobial action in bacteria and proliferative action in human skin cells because of the better contact of cells with the surfaces and more efficient stimuli transfer.

Following the concept of improving the piezoelectric properties of PLLA by incorporating morphologically anisotropic filler particles,[9] rod-like ZnO NPs were explored as fillers. After integration into the PLLA bulk, the ZnO nanorods were very homogeneously distributed within the polymer matrix. Owing to their nanometre size, their morphological anisotropy was not high enough to enable oriented crystallization of PLLA, as was previously observed for micrometre-long fillers.[9] However, the evenly distributed filler within the polymer matrix did affect the crystalline phase of PLLA and promoted partial crystallization of PLLA into a thermodynamically more stable and more arranged α-phase, which affected its long-range ordering.

More significantly, the presence of homogeneously distributed ZnO NPs within the PLLA matrix played an important role in their activation with US and affected the resulting piezoelectric properties. Sonication was previously shown to improve the functional properties of piezocomposites that contained poled inorganic piezoelectric particles that were activated with US within a polymeric matrix.[26] Here, the effect was the opposite. Nonpoled small filler particles increased the piezoelectric response of the polymeric matrix rather than contributing to its own piezoelectric response. Previously, the presence of ZnO in PLLA was observed to increase the piezoelectric response of PLLA, which was a conse-

quence of the formation of the β-PLLA phase within electrospun PLLA ZnO fibres.[27] However, as the filler was unable to induce oriented crystallization or promote a highly ordered β-PLLA phase, its influence on the piezoelectric response could be explained by its contribution to the mechanical deformation of the polymer. During interactions with US waves, both the matrix and the filler were affected. As the filler particles were small and well distributed within the matrix, their mobility inside the polymer was not significantly inhibited by the matrix, and they intensely vibrated inside the film. Consequently, the mechanical deformation, which affected the PLLA matrix, was a result of coupling of the interactions of the US waves and the polymer matrix as well as mechanical deformation that was induced by filler particles vibrating inside the matrix. Previously, laminated, flexible structures made of components with different mechanical properties (i.e., different elasticities) were predicted to be deformed by US primarily by shear deformation.[28] The force that generates shear is generated at the interface between the two mechanically mismatched structures. As an analogue, the PLLA matrix and incorporated ZnO fillers could be understood as mechanically mismatched structures. The shear deformation at their interface increases the piezoelectric response of the PLLA matrix. Consequently, compared with the absence of filler,

increased mechanical deformation increased the piezoelectric response of the PLLA ZnO. The increase was larger with a higher filler content.

Plasma added new functional groups to the PLLA surface mainly because of oxidation that was induced by reactive oxygen-containing species and, to a lesser extent, nitrogen-containing species. In addition, surface etching removed thin layers of the polymeric matrix and partially revealed ZnO NP fillers from the bulk material. This increased the amount of ZnO that was available at the surfaces of the plasma-treated films. Changes in surface chemistry directly affected the wettability of the films and significantly increased their hydrophilicity. The final wettability of each plasma-treated surface was a combination of increased hydrophilicity due to the plasma-oxidized PLLA groups and increased hydrophobicity due to ZnO fillers that were partially released at the surface.

Although ZnO is intrinsically polar and hydrophilic, increasing the ZnO content led to higher apparent hydrophobicity after plasma treatment. This behaviour is attributed to accelerated hydrophobic recovery of the PLLA surface. Plasma initially introduces polar functional groups and increases surface hydrophilicity; however, this effect is transient due to polymer chain reorientation and migration of low-energy segments.[29,30] It seems that the presence of a polar ZnO filler likely promotes interactions with plasma-induced polar groups and facilitates surface rearrangement, resulting in preferential exposure of nonpolar PLLA segments and an apparent partial increase in hydrophobicity at higher ZnO loadings. Consequently, the surface properties, including chemistry, wettability and roughness, were adjusted for more intensive interactions with cells, including both initial adhesion and stimulus transfer.

In the case of interactions with bacterial cells, both the ZnO NP filler-induced increase in the piezoelectricity and the plasma-assisted increase in the ZnO content at the surface were found to increase antimicrobial activity (which suggests that their individual antimicrobial actions were very modest and quite slow). Interestingly, the modest antimicrobial action of the ZnO NPs and the slow antimicrobial action of piezostimulation using piezo-PLLA were combined into the significantly more efficient and faster antimicrobial action of the piezo-PLLA/ZnO structures. This increase was confirmed not to be a consequence of the release of the ZnO filler or indirectly formed active components, such as ROS, as their contents were too low to affect bacterial cells. Zeta potential measurements revealed that the ZnO NPs are cationic. At pH values between 7 and 9, Zn^{2+} and $Zn(OH)^+$(aq) ions dominate, thereby resulting in a positive zeta potential.[11,24] In addition, the bacteria were not affected by US or PLLA ZnO films without US stimulation. However, their stimulation at the surfaces of US-activated piezoelectric PLLA ZnO films resulted in antimicrobial activity, which depended on the content of the ZnO NP filler. In terms of the US-generated voltage output, compared with pure PLLA, both ZnO NP filler-containing PLLA films had significantly higher values. On the other hand, the difference in the voltage between 1 wt% PLLA and 6 wt% PLLA ZnO was not statistically significant. Nevertheless, this difference in voltage produced a

difference in antimicrobial action. Specifically, whereas the 200 mV material that was produced with pure PLLA was not active, the 300 mV material that was produced with 1 wt% PLLA was bacteriostatic, and the 400 mV material that was produced with 6 wt% PLLA was bactericidal. Bacteria have a negative net surface charge because of functional groups in the cell membrane, phospholipids in Gram-positive strains and teichoic acids in Gram-negative strains.[11] Therefore, the ZnO NP filler, which was partially revealed at the surface after plasma treatment, plays an important role, as it contributes to better bacterial adhesion. This is the critical step for signal transfer during US-activated piezostimulation. In the contact killing of bacteria, ion interactions occur between the cell membrane and the charged surface of the polymer, which leads to a breakdown of the transmembrane potential. The dipole moment at the US-activated surface of the polymer and the generated electric field affect the components of the cell membrane, thereby leading to deformation and lysis of bacteria that are attached to the polymer, as was observed earlier.[3] Owing to better cell adhesion and more effective stimulus transfer, the modification particularly increased the rate and efficacy of the antimicrobial action of the piezostimulant.

In the second stage, the interactions were tested in human cells using human keratinocytes. Owing to the modest antimicrobial action of free ZnO NPs, they were found to have cytotoxic effects at concentrations close to those that enabled antimicrobial action (IC > 400 μg ml^{-1} and MIC > 300 μg ml^{-1}), thus providing a narrow therapeutic window. However, after they were integrated into the films, the antimicrobial activity rapidly increased because of the synergy with piezostimulation, and much lower concentrations of ZnO were needed to ensure effective action against bacteria. The design of a PLLA ZnO film in which the filler particles are well integrated into the bulk and only partially exposed to the surface after plasma treatment provides a very effective solution. In this way, the particles were available for interactions with bacteria, but their uncontrolled release was prevented. Consequently, the ZnO NPs in PLLA did not induce cytotoxic effects in human cells. Moreover, the surface changes in the films that were induced by the plasma treatment improved the adhesion of human cells directly onto the surfaces of the films. Additional piezostimulation of adhered cells positively affected their cytoskeletons, promoted cell elongation and increased their connectivity, which contributed to better coverage of the surface and cell proliferation, thereby leading to improved cell density, which is very important for the regeneration and healing of wounds.

Notably, the effect of piezostimulation on the morphology of human cells clearly revealed that they were sensing the stimuli and responding to them. Previously, we reported that HaCaT cells were morphologically polarized and oriented towards the drawing direction of the polymer, which matched the direction of the piezo PLLA dipole orientation.[9] Here, we report that cells respond to piezostimuli through the extensive formation of cellular protrusions in the form of filopodia and lamillopodia. Both are known as motile organelles known for their roles in cell migration and at adhesion sites, and filopo-

dia also play a role as sensory organelles in the exploration of the external environment and probing cues.[31,32] Very similar profound formation of filopodia was detected in osteoblasts that were piezostimulated and adhered to the surfaces of poly-vinylidene fluoride (PVDF) films, which also produced increased amounts of extracellular collagen matrix for biomi-neralization.[33] In neural cells, their formation can be triggered by increased local levels of intracellular Ca^{2+}, which recruits Cobl and causes its local accumulation as an important mediator of dendritic cellular protrusions, which is then fol-lowed by the formation of actin patches at their sites.[34,35] In HaCaT cells, filopodia are associated not only with the sensing environment but also with the formation of adhesion sites that are responsive to the accurate movement, direction of move-ment and localization of adhesion sites.[36] The mechanism of piezostimulation and interactions between HaCaT cells and the electrostimulating substrate on which they are adhered, grown and spread is not completely clear. Extensive filopodia gene-ration could be associated with their sensing function, detec-tion and response to electrical cues during piezostimulation, which trigger the formation of these cellular protrusions and promote their elongation to the particular point where electro-stimulating stimuli are present. Actin filaments, which are known as tensor sensors,[37] certainly respond to mechanical deformations that are induced by activation with US. However, as polar structures inside filopodia, they might also be involved as electrical dipole sensors, which will be very interesting to explore in more detail in the future.

The application of US-activated piezoelectric films shows promise as advanced regeneration technology. The integration of the antimicrobial filler increases the piezoelectricity of the films and reinforces the kinetics of their antimicrobial action. Consequently, the non-selective and non-specific disintegration of the bacteria, obtained during piezostimulation, would effectively eliminate infection and, most importantly, not leave bacteria an option to develop resistance. In conjunction with the enhance-ment of the cell proliferation and regeneration, the piezostimula-tion is expected to contribute particularly to the treatment of slowly regenerating tissues, including chronic wounds.

Conclusions

ZnO NPs are a very effective filler that improves the US-acti-vated piezoelectric response of PLLA films and modifies their surface chemistry after plasma treatment. These modifications synergistically tailor the interactions of piezo-PLLA films with cells during piezostimulation, which consequently increases the efficacy of antimicrobial action and promotes human cell proliferation.

Author contributions

ŠŠ: investigation, visualization, and writing – original draft; MŽ: investigation, visualization, formal analysis, and writing – review

and editing; LG: investigations, validation, and writing – review and editing; MSS: investigations; IJ: resources and writing – review and editing; TR: investigations; MP: investigations and writing – review and editing; MŠ: formal analysis and writing – review and editing; MS: writing – review and editing and funding acquisition; MV: conceptualization, visualization, writing – review and editing, funding acquisition, and supervision.

Conflicts of interest

There are no conflicts to declare.

Data availability

We confirm that all source files related to the information pro-vided in this manuscript are deposited and publicly available in Zenodo at https://doi.org/10.5281/zenodo.17256748.

Supplementary information (SI): SAXS analysis, water contact angle of ZnO NPs, SEM investigation of the surface and effect of the Zn^{2+} ions to bacterial growth. See DOI: https://doi.org/10.1039/d5bm01497b.

Acknowledgements

References

1 E. O. Carvalho, *et al.*, Tailoring Bacteria Response by Piezoelectric Stimulation, *ACS Appl. Mater. Interfaces*, 2019, **11**, 27297–27305.

2 S. K. Ahmed, *et al.*, Antimicrobial resistance: Impacts, chal-lenges, and future prospects, *J. Med. Surg. Public Health*, 2024, **2**, 100081.

3 L. Gazvoda, M. Perišić Nanut, M. Spreitzer and M. Vukomanović, Antimicrobial activity of piezoelectric polymer: piezoelectricity as the reason for damaging bac-terial membrane, *Biomater. Sci.*, 2022, **10**, 4933–4948.

4 X. Yang, *et al.*, Piezoelectric nanomaterials for antibacterial strategies, *Appl. Mater. Today*, 2024, **40**, 102419.

5 L. Udovč, M. Spreitzer and M. Vukomanović, Towards hydrophilic piezoelectric poly-L-lactide films: optimal pro-cessing, post-heat treatment and alkaline etching, *Polym. J.*, 2020, **52**, 299–311.

6 C. Zhi, *et al.*, Recent Progress of Wearable Piezoelectric Pressure Sensors Based on Nanofibers, Yarns, and Their Fabrics via Electrospinning, *Adv. Mater. Technol.*, 2023, **8**, 2201161.

7 M. Smith, *et al.*, Poly-L-Lactic Acid Nanotubes as Soft Piezoelectric Interfaces for Biology: Controlling Cell Attachment via Polymer Crystallinity, *ACS Appl. BIO Mater.*, 2020, **3**, 2140–2149.

8 M. Ando, S. Takeshima, Y. Ishiura, K. Ando and O. Onishi, Piezoelectric antibacterial fabric comprised of poly(l-lactic acid) yarn, *Jpn. J. Appl. Phys.*, 2017, **56**, 10PG01.

9 M. Vukomanović, *et al.*, Filler-Enhanced Piezoelectricity of Poly-L-Lactide and Its Use as a Functional Ultrasound-Activated Biomaterial, *Small*, 2023, **19**, 2301981.

10 I. Kim, *et al.*, ZnO Nanostructures in Active Antibacterial Food Packaging: Preparation Methods, Antimicrobial Mechanisms, Safety Issues, Future Prospects, and Challenges, *Food Rev. Int.*, 2022, **38**, 537–565.

11 W. J. Chong, *et al.*, Biodegradable PLA-ZnO nanocomposite biomaterials with antibacterial properties, tissue engineering viability, and enhanced biocompatibility, *Smart Mater. Manuf.*, 2023, **1**, 100004.

12 X. Pan, *et al.*, Immunomodulatory zinc-based materials for tissue regeneration, *Biomater. Adv.*, 2023, **152**, 213503.

13 L. Gazvoda, B. Višić, M. Spreitzer and M. Vukomanović, Hydrophilicity affecting the enzyme-driven degradation of piezoelectric poly-l-lactide films, *Polymers*, 2021, **13**, 1719.

14 Q. Cheng, B. L. P. Lee, K. Komvopoulos, Z. Yan and S. Li, Plasma surface chemical treatment of electrospun poly (L-lactide) microfibrous scaffolds for enhanced cell adhesion, growth, and infiltration, *Tissue Eng., Part A*, 2013, **19**, 1188–1198.

15 P. Seleš, *et al.*, Altering defect population during the solvo-thermal growth of ZnO nanorods for photocatalytic applications, *Ceram. Int.*, 2024, **50**, 26819–26828.

16 J. T. Van Elteren, V. S. Šelih and M. Šala, Insights into the selection of 2D LA-ICP-MS (multi)elemental mapping conditions, *J. Anal. At. Spectrom.*, 2019, **34**, 1919–1931.

17 J. T. van Elteren, M. Šala and D. Metarapi, Comparison of single pulse, multiple dosage, and 2D oversampling/deconvolution LA-ICPMS strategies for mapping of (ultra)low-concentration samples, *Talanta*, 2021, **235**, 122785.

18 M. Vukomanovic and E. Torrents, High time resolution and high signal-to-noise monitoring of the bacterial growth kinetics in the presence of plasmonic nanoparticles, *J. Nanobiotechnol.*, 2019, **17**, 21.

19 E. Pinho, L. Magalhães, M. Henriques and R. Oliveira, Antimicrobial activity assessment of textiles: Standard methods comparison, *Ann. Microbiol.*, 2011, **61**, 493–498.

20 V. N. Kalpana, *et al.*, Biosynthesis of zinc oxide nanoparticles using culture filtrates of Aspergillus niger: Antimicrobial textiles and dye degradation studies, *OpenNano*, 2018, **3**, 48–55.

21 K. Jariyavidyanont, A. Janke, Q. Yu, T. Thurn-Albrecht and R. Androsch, Lamellar Morphology of Disorder α′-Crystals of Poly(L-Lactic Acid), *Cryst. Growth Des.*, 2024, **24**, 1825–1834.

22 K. Billimoria, E. L. Heeley, N. Parsons and Ł. Figiel, An investigation into the crystalline morphology transitions in poly-L-lactic acid (PLLA) under uniaxial deformation in the quasi-solid-state regime, *Eur. Polym. J.*, 2018, **101**, 127–139.

23 R. Schönlein, *et al.*, The Combined Effects of Optical Purity, Chain Orientation, Crystallinity, and Dynamic Mechanical Activation as Means to Obtain Highly Piezoelectric Polylactide Materials, *ACS Appl. Polym. Mater.*, 2024, **6**, 7561–7571.

24 M. Dembek, S. Bocian and B. Buszewski, Solvent Influence on Zeta Potential of Stationary Phase—Mobile Phase Interface, *Molecules*, 2022, **27**, 968.

25 M. Vukomanovic, M. M. del Cendra, A. Baelo and E. Torrents, Nano-engineering stable contact-based antimicrobials: Chemistry at the interface between nano-gold and bacteria, *Colloids Surf., B*, 2021, **208**, 112083.

26 X. Lei, *et al.*, Ultrasound–Driven Piezoelectric Strategy and Performance: Polyurethane–Based Functioning Networks in Actuating Bone Repair, *Adv. Funct. Mater.*, 2025, **35**, 2502684.

27 M. Xu, *et al.*, Flexible piezoelectric generator based on PLLA/ZnO oriented fibers for wearable self-powered sensing, *Composites, Part A*, 2023, **169**, 107518.

28 S. Li, X. Liu, R. Li and Y. Su, Shear deformation dominates in the soft adhesive layers of the laminated structure of flexible electronics, *Int. J. Solids Struct.*, 2017, **110–111**, 305–314.

29 V. Luque-Agudo, M. Hierro-Oliva, A. M. Gallardo-Moreno and M. L. González-Martín, Effect of plasma treatment on the surface properties of polylactic acid films, *Polym. Test.*, 2021, **96**, 107097.

30 M. Mortazavi and M. Nosonovsky, A model for diffusion-driven hydrophobic recovery in plasma treated polymers, *Appl. Surf. Sci.*, 2012, **258**, 6876–6883.

31 P. K. Mattila and P. Lappalainen, Filopodia: Molecular architecture and cellular functions, *Nat. Rev. Mol. Cell Biol.*, 2008, **9**, 446–454.

32 K. Rottner and T. E. B. Stradal, Actin dynamics and turnover in cell motility, *Curr. Opin. Cell Biol.*, 2011, **23**, 569–578.

33 P. K. Szewczyk, *et al.*, Enhanced osteoblasts adhesion and collagen formation on biomimetic polyvinylidene fluoride (PVDF) films for bone regeneration, *Biomed. Mater.*, 2019, **14**, 065006.

34 G. Leondaritis and B. J. Eickholt, Short Lives with Long-Lasting Effects: Filopodia Protrusions in Neuronal Branching Morphogenesis, *PLoS Biol.*, 2015, **13**, e1002241.

35 W. Hou, *et al.*, The Actin Nucleator Cobl Is Controlled by Calcium and Calmodulin, *PLoS Biol.*, 2015, **13**, e1002233.

36 C. Schäfer, *et al.*, One step ahead: Role of filopodia in adhesion formation during cell migration of keratinocytes, *Exp. Cell Res.*, 2009, **315**, 1212–1224.

37 V. E. Galkin, A. Orlova and E. H. Egelman, Actin filaments as tension sensors, *Curr. Biol.*, 2012, **22**, R96–R101.